Synthesis and microwave absorption properties of Ni0.5Zn0.5Fe2O4/Cl composite coated with polyaniline within paraffin wax matrix

anas houbi (anashoubi@gmail.com)
Al-Farabi Kazakh National University
Zharmenov Aldashevich
Yomen Atassi
Zhenisgul Telmanovna
MIRZALIEVA Saule

Research Article

Keywords: NiZn ferrite, PANI, Lightweight microwave absorber, Reflection loss, Absorption bandwidth

Posted Date: May 19th, 2022

DOI: https://doi.org/10.21203/rs.3.rs-1637416/v1

Synthesis and microwave absorption properties of $Ni_{0.5}Zn_{0.5}Fe_2O_4$/CI composite coated with polyaniline within paraffin wax matrix

Anas Houbi[1*], Yomen Atassi[2], Zharmenov Abdurassul Aldashevich[1], Bagasharova Zhenisgul Telmanovna[1], Mirzalieva Saule[1]

[1]Department of Complex Processing of Mineral Raw Materials, Al-Farabi Kazakh National University, 050044 Al-Farabi, Kazakhstan
[2]Department of Applied Physics, Higher Institute for Applied Sciences and Technology, Damascus, Syria
*Author for correspondence (anashoubi@gmail.com)

Abstract:

In this paper, Ternary composites of polyaniline/NiZn ferrite/carbonyl iron (PANI/F/CI) are prepared via two stages: Firstly, $Ni_{0.5}Zn_{0.5}Fe_2O_4$ is prepared using a sol-gel method while carbonyl iron is commercially purchased. After that, PANI/F/CI composites are prepared using an in-situ polymerization technique of PANI in the existence of the $Ni_{0.5}Zn_{0.5}Fe_2O_4$ and CI. X-ray diffractometry, FTIR spectroscopy, UV-vis spectroscopy, TGA analysis, and SEM analysis are utilized in order to characterize samples. The morphology of the powders is investigated by SEM. The electromagnetic interference shielding and microwave absorption properties are measured in the frequency band of 8.8–12 GHz to investigate the microwave characterization. The results refer those microwave absorption properties are related to the absorber thickness and the loading ratio of the absorber within a paraffin matrix. Minimal reflection loss of -30.8 dB at the matching frequency of 10.3 GHz and the absorption bandwidth under -10 dB of 2.8 GHz for 3.4 mm thickness with a surface density of 3.38 kg/m^2 are noticed for the PANI/F/CI composite sample. The maximum shielding efficiency of 30.12 dB at 11.0 GHz for 3.2 mm thickness is observed for the PANI/F/CI composite sample.

Keywords: NiZn ferrite, PANI, Lightweight microwave absorber, Reflection loss, Absorption bandwidth.

1. Introduction

Recent environmental pollution issues are appearing because of the quick evolution of electronic devices, involving smartphones, laptops, and intelligent devices. Electronic apparatuses emit undesirable EM waves, generating electromagnetic interference (EMI) between various electronic apparatuses with a negative effect on their performance. Consequently, the disposal of EM waves resulting from EMI effectively is so important both for public protection security and electronic safety [1–6]. Generally, there are two kinds of materials to absorb EM waves: firstly, is magnetic loss materials such as hexagonal ferrites, spinel ferrites, and carbonyl iron, secondly, is dielectric loss materials such as conductive polymers (e.g., polyaniline, polypyrrole) and carbonaceous materials (e.g., carbon black, activated carbon, carbon fibers,

graphene) which have played a significant role for high-frequency EM wave absorption. Nevertheless, the drawbacks involving elevated density, low reflection absorption, and narrow wideband have hugely limited conventional loss materials' workable benefits for EM wave absorption [7–10]. In recent years, microwave absorption (MA) composites based on polyaniline, ferrite and carbonyl iron, have obtained significant attention due to their excellent electrical and ferrimagnetic characteristics. Polyaniline-based composites have pulled in major attention for microwave absorption lately. Polyaniline is usually used to fit the requirements of high-effective microwave attenuation materials because of its superior characteristics, for example, low density, high permittivity, unique electronic conductivity, etc. Polyaniline has a unique place in the band of elevated-frequency MAMs. Furthermore, spinel ferrites and carbonyl iron have excellent MA characteristics due to their unique magnetic characteristics. NiZn ferrites and carbonyl iron are considered suitable materials for high-frequency implementations [11,12]. When NiZn ferrite and carbonyl iron are mixed with Polyaniline, the MA characteristics of the resultant composite are anticipated to enhance. According to this, PANI/NiZn ferrite microwave absorbers in the frequency range of 2–40 GHz were successfully prepared by Jau et al. [11]. The absorbers are prepared by dispersing PANI/NiZn ferrite nanocomposites with a weight ratio of 67% w/w within an epoxy resin matrix. The results indicated that by increasing polyaniline content in NiZn ferrite, a wide absorption frequency range could be obtained. Ali et al. have designed microwave absorbers in the frequency band of 8-12 GHz based on PANI/MnNiZn ferrite at the weight ratio of 1:1. The absorbers are formed by dispersing PANI/MnNiZn ferrite within a paraffin matrix of 20–25% w/w. The results have shown that the absorber with a loading percentage within a paraffin matrix of 25% w/w had a minimum reflection loss (RL_{min}) of -31.32 dB at 11.13 GHz and the absorption bandwidth under -10 dB (BW_{-10dB}) was 3.74 GHz for 3 mm thickness [13]. Xie et al. have reported the MA properties of a one-dimensional uniform PANI/NiZn ferrite hybrid nanorods within a paraffin matrix of 70% w/w in the frequency range of 2-18 GHz. They have found that the absorbers had broadband, and minimal reflection loss, where the results have indicated that the absorber had a RL_{min} of -27.5 dB at 6.2 GHz and the absorption BW_{-10dB} was 3 GHz for 2 mm thickness [14]. Zhang et al. have prepared PANI/NiZn ferrite composites by in-situ polymerization within a paraffin matrix of 75% w/w. The molar ratios of PANI/NiZn ferrite were 3:1, 2:1, 1:1, 1:2, 1:3, where the optimal sample has exhibited PANI/NiZn at the molar ratio of 1:2 had a RL_{min} of -41 dB at 12.8 GHz and the absorption BW_{-10dB} was 5 GHz for 2.6 mm thickness [15]. Until now, to the best of our knowledge, no studies have been reported on the EMI shielding and MA properties of composites made up of polyaniline/NiZn ferrite/carbonyl iron. In this paper, a perfect absorber is obtained by incorporating $Ni_{0.5}Zn_{0.5}Fe_2O_4$ and CI (magnetic loss materials) and PANI (dielectric loss material) within a paraffin wax matrix. Where we study the effect of different absorber thicknesses and the loading ratio of the absorber within a paraffin matrix on the microwave absorption behavior. The preparation of such composites is verified by different characterization methods involving X-ray diffractometry, FTIR spectroscopy, UV-vis spectroscopy, TGA analysis, and SEM analysis. The EMI shielding and MA

properties are studied by measuring the RLmin, BW_{-10dB}, and SE of the absorbers in the frequency band of 8.8–12 GHz to achieve functional characterization.

2. Experimental procedure

2.1 Synthesis of NiZn ferrite and carbonyl iron powders

Ferrite ($Ni_{0.5}Zn_{0.5}Fe_2O_4$) nanoparticles were prepared by a sol-gel method. $Ni_{0.5}Zn_{0.5}Fe_2O_4$ nanoparticles were synthesized by taking appropriate amounts of nickel(II) nitrate hexahydrate ($Ni(NO_3)_2{\cdot}6H_2O$), zinc nitrate hexahydrate ($Zn(NO_3)_2{\cdot}6H_2O$) and iron(III) nitrate nonahydrate ($Fe(NO_3)_3.9H_2O$) were blended together and with citric acid (1 mole per metal ion), then the whole mixture pH value was modified to 7.0 using NH_4OH. The whole mixture was put onto a hot plate with constant stirring at 90 °C for 6 h to shape the viscous gel. Then, the viscous gel was transferred to the oven for drying for 2 h at 200 °C to obtain a fluffy carbonaceous pyrolyzed mass. After that, the resulting mass was annealed for 4 h at 650 °C to obtain nanoparticles of ferrite. On the other hand, carbonyl iron was purchased from Cabot Corporation Company. The average particle size of carbonyl iron powder was measured utilizing the sieve shaker and it was between 10-25 μm. Carbonyl iron powder was milled for 12 h at 300 rpm via the grinding balls to obtain fine powders.

2.2 Preparation of PANI/F /CI

NiZn ferrite and carbonyl iron were coated with polyaniline via the in-situ polymerization technique. Firstly, 6 g (90%F and 10%CI) was added to 100 ml distilled water under mechanical stirring at a speed of 250 rpm for 30 minutes. 3 g sodium dodecyl sulfate (SDS) and aniline were added to the solution while keeping mechanical stirring for 1 h. After that, 1 M HCl solution 80 mL was added to the solution under stirring for 1 h. Finally, 8.5 g APS was dissolved in 100 ml of an aqueous solution which was utilized as an oxidizing agent and added slowly dropwise into the solution to start the polymerization. The polymerization was allowed to proceed for 6 h with stirring in an ice bath. The resulting composite was filtered and washed many times with distilled water and ethanol, and then dried for 8 h in the furnace at 70 °C. The weight ratio of aniline/(F-CI) (1/1) was synthesized. Pure polyaniline was synthesized in a similar way but without NiZn ferrite and carbonyl iron solution for comparison purposes.

2.3 Preparation of samples for measuring the MA and EMI shielding properties

Microwave absorption and electromagnetic interference shielding properties of the samples were estimated with the free-space technique. According to this, 30-35% w/w of the coated composites were dispersed in a paraffin wax matrix by heating and stirring for 15 min. Thereafter, the single-layer samples were

molded to the dimensions of 100×100 mm to measure RL and SE in the frequency band of 8.8–12 GHz.

2.4 Measurements

A powder X-ray diffractometer (XRD, Rigaku Miniflex 600, Cu-Ka) is utilized for defining the crystal structures of the powders. Fourier Transform IR (FTIR) spectra are recorded on a Perkin Elmer spectrum 65 FTIR spectrometer in the range of 400–4000 cm^{-1}. The UV–vis absorption spectra of the samples (dispersed in dimethylformamide (DMF)) are recorded using the LAMBDA 365 UV–vis spectrophotometer in the range of 250–900 nm. Thermogravimetric analysis (TGA) is done utilizing a thermal analyzer (NETZSCH 449F3A-0372-M) under a nitrogen atmosphere, from room temperature to 1000°C under a constant heating rate of 10 °C/min. A scanning electron microscope (FEI Quanta 200 3D) is utilized for defining the morphology of the powders. The EMI shielding and MA properties of the prepared samples are measured by using the horn antenna connected to an oscilloscope.

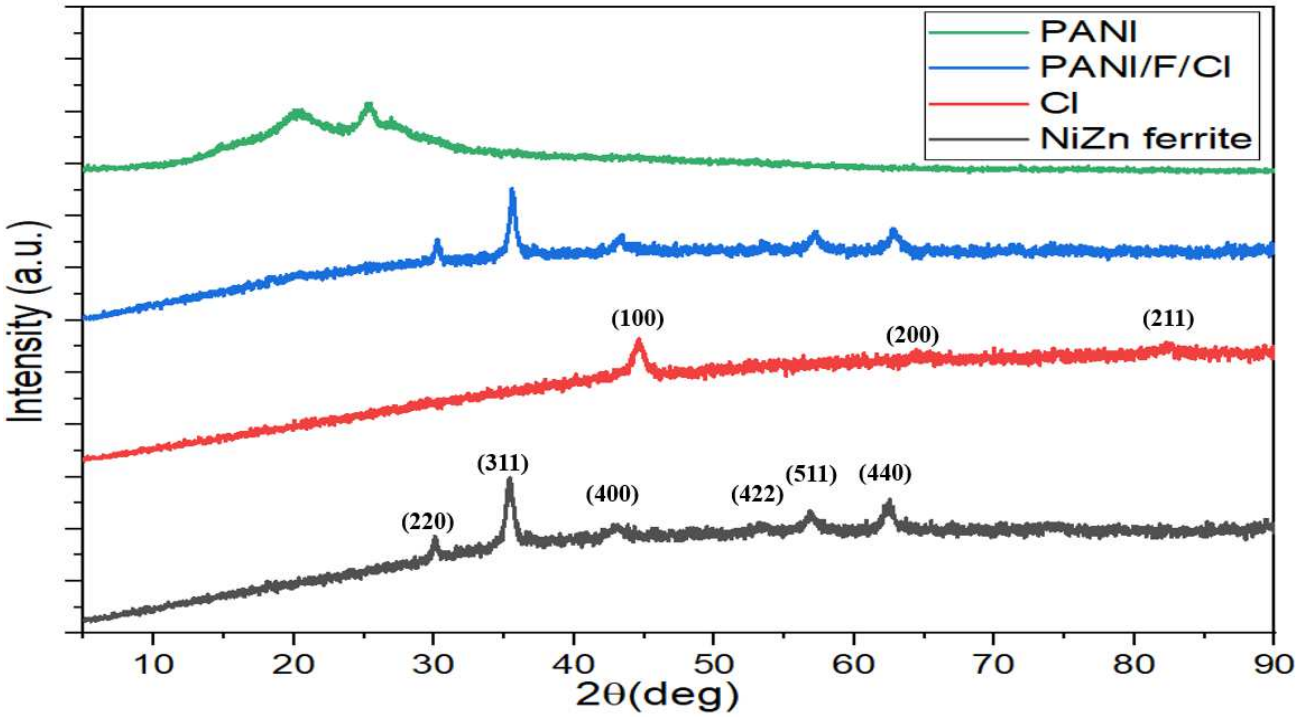

Fig. 1. XRD patterns of $Ni_{0.5}Zn_{0.5}Fe_2O_4$, CI, PANI/F/CI composite and pure PANI.

3. Results and discussion

3.1 XRD patterns

The crystalline structures of the prepared samples are identified by XRD. The XRD patterns of $Ni_{0.5}Zn_{0.5}Fe_2O_4$, CI, PANI/F/CI composite and PANI are shown in Fig. 1. For the $Ni_{0.5}Zn_{0.5}Fe_2O_4$ pattern, six diffraction peaks are noticed at 2θ values of 30.04°, 35.44°, 43.12°, 53.68°, 57.18°, and 62.14°, which conforms to (hkl) planes of (220), (311),

(400), (422), (511) and (440), respectively. The ideal spinel structure is noticed by the peaks of NiZn ferrite [16]. The XRD pattern of $Ni_{0.5}Zn_{0.5}Fe_2O_4$ is totally matched with the reference XRD patterns (JCPDS, PDF no. 08–0234). The size of the NiZn ferrite grain (2θ =35.44°) has been evaluated with Scherrer's equation, $D=0.9\ \lambda/\beta\ \cos\theta$, where D is the crystallite size (nm), λ is the X-ray wavelength, β is the bandwidth at half-height, and θ is the diffraction angle in degree. The calculated crystallite size of the NiZn ferrite is 27.6 nm. On the other hand, for the carbonyl iron pattern, three characteristic peaks are noticed at 2θ values of 44.61°, 64.92° and 82.33°, which conform to (hkl) planes of (100), (200), and (211), respectively. The XRD pattern of carbonyl iron resembles crystallites in which the sample mainly contains α-Fe phase [17]. All the observed peaks of CI are matched with the standard XRD pattern (JCPDS, PDF no. 06-0696). The characteristic peaks of the PANI/F/CI composite show matching the characteristic peaks of $Ni_{0.5}Zn_{0.5}Fe_2O_4$ as mentioned above. The XRD pattern of the pure PANI (Fig. 1) displays an amorphous structure with two characteristic peaks at 20.22° and 25.36° which are attributed to the periodicity parallel to the polymer chains of PANI [18,19]. The XRD patterns of the PANI/F/CI composite (Fig. 1) display crystalline peaks because of the existence of NiZn ferrite in this composite. The two characteristic peaks of the PANI disappeared due to the $Ni_{0.5}Zn_{0.5}Fe_2O_4$ nanoparticles [20,21].

3.2 FTIR spectra

Fig. 2 shows the FTIR spectra of the $Ni_{0.5}Zn_{0.5}Fe_2O_4$, CI, PANI/F/CI composite and PANI. For the $Ni_{0.5}Zn_{0.5}Fe_2O_4$ nanoparticles, two peaks at 563.1 cm^{-1} and 430.2 cm^{-1} are referring to the stretching vibration of (Fe-O), which emphasizes the formation of the metal-oxygen in ferrite-based [22]. In addition to that, the peak at 1630.4 cm^{-1} in $Ni_{0.5}Zn_{0.5}Fe_2O_4$, and CI is referring to C=O stretching vibration, and the peaks at 2348 cm^{-1} and 3452 cm^{-1} are referring to O-H stretching vibration [23,24]. On the other hand, the characteristic peaks of PANI and PANI/F/CI composite are similar and they exhibited peaks at 1568 cm^{-1}, 1489 cm^{-1}, 1298 cm^{-1}, 1238 cm^{-1}, 1113 cm^{-1}, and 800 cm^{-1} [25,26]. The characteristic peaks at 1568 and 1489 cm^{-1} are attributed to the C=N and C=C stretching modes of vibration for the quinonoid and benzenoid units of the polymer. The characteristic peaks at 1298 and 1238 cm^{-1} are related to N-H bending and asymmetric C-H stretching of the benzenoid ring, respectively. Finally, the characteristic peaks at 1113 cm^{-1} and 800 cm^{-1} are ascribed to the vibration mode of N=Q=N and the out-of-plane stretching vibration of C–H, respectively [15,20]. In addition to that, the characteristic peak at 563.1 cm^{-1} of PANI/F/CI composite

shows matching the characteristic peak of $Ni_{0.5}Zn_{0.5}Fe_2O_4$ as mentioned above. This indicates the stretching vibration of (Fe-O), which confirms the formation of the metal-oxygen in PANI/F/CI.

3.3 UV–visible spectra

The UV–visible spectrum of the PANI and PANI/F/CI composite is shown in Fig. 3. For PANI, two characteristic peaks at around 302 nm and 629 nm are observed. The characteristic peak around 302 nm is ascribed to π–π* transition of the benzenoid ring and the characteristic peak around 629 nm is attributed to the benzenoid-to-quinoid excitonic transition [18,27]. It can be seen from Fig. 3 that the characteristic peaks of PANI/F/CI composite show a clear red shift of 7 nm, as compared with that of polyaniline. The two characteristic peaks show the presence of PANI on the surface of $Ni_{0.5}Zn_{0.5}Fe_2O_4$ and carbonyl iron. These results may refer to the σ–π interaction among $Ni_{0.5}Zn_{0.5}Fe_2O_4$, carbonyl iron and polyaniline backbone, which leads to the energy of the antibonding orbital decrease, the energy of the π–π* transition of the benzenoid and quinoid ring decreases, so the characteristic peaks of the composite show a red shift [27].

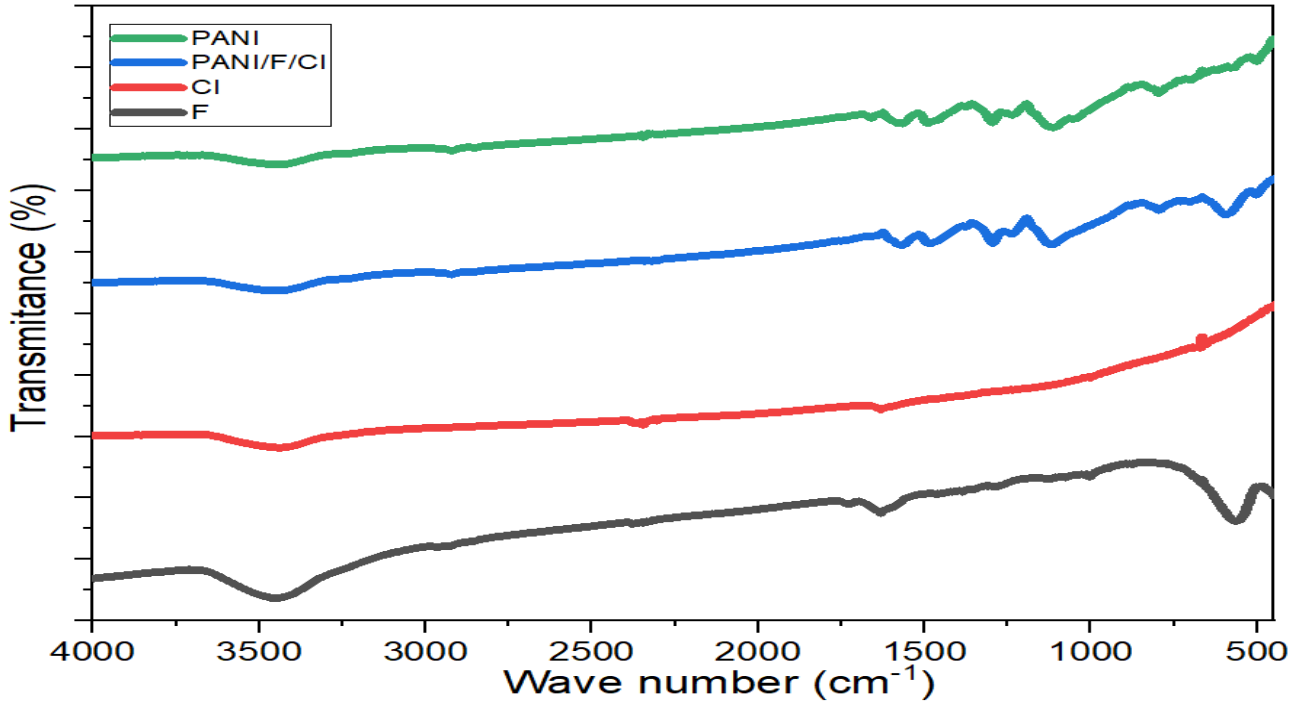

Fig. 2. FTIR spectra of $Ni_{0.5}Zn_{0.5}Fe_2O_4$, CI, PANI/F/CI composite and pure PANI.

3.4 TGA analysis

The TGA curves of the $Ni_{0.5}Zn_{0.5}Fe_2O_4$, PANI/F/CI composite and PANI are shown in Fig. 4. For the $Ni_{0.5}Zn_{0.5}Fe_2O_4$ nanoparticles, no mass loss was noticed over the whole temperature range. PANI loses 4.87% of its weight in the range of 110–130 °C which is due to the evaporation of moisture in the PANI.

The thermal decomposition of the PANI is shown in the range of 230–1000 °C and has a big weight loss of 65.12%. On the other hand, PANI/F/CI composite loses about 2.21% of their weight in the range of 110–130 °C which is due to the evaporation of moisture in the composite. The thermal decomposition of the PANI/F/CI composite is shown in the range of 240–870 °C and has a big weight loss of 46.28%.

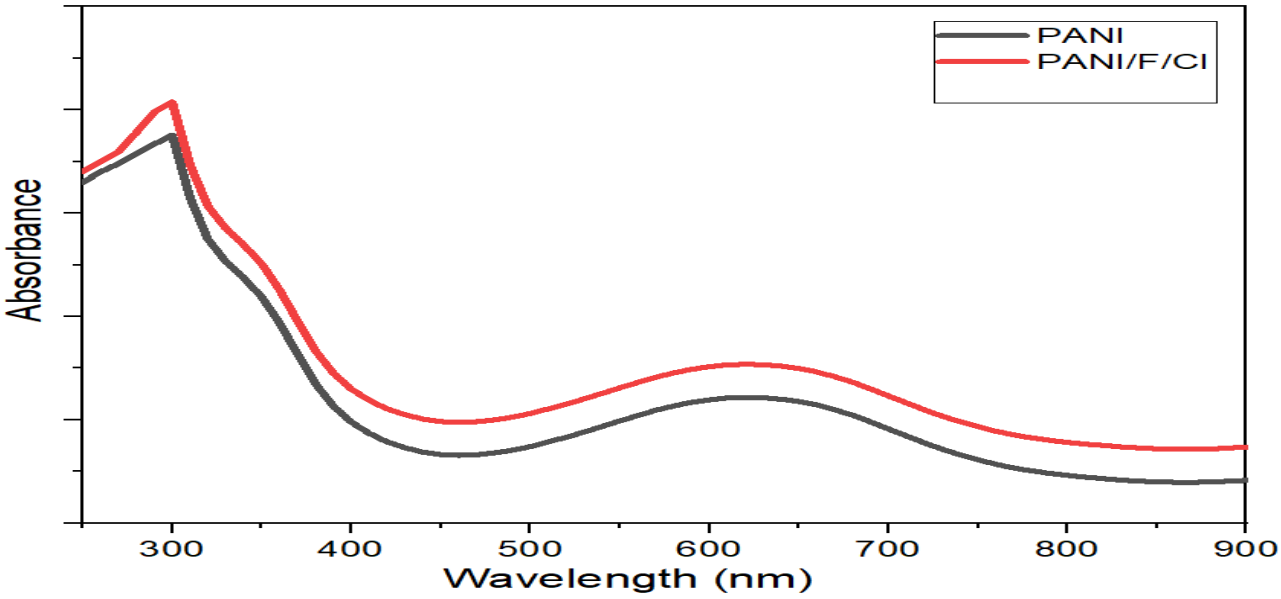

Fig. 3. UV spectra of PANI and PANI/F/CI composite.

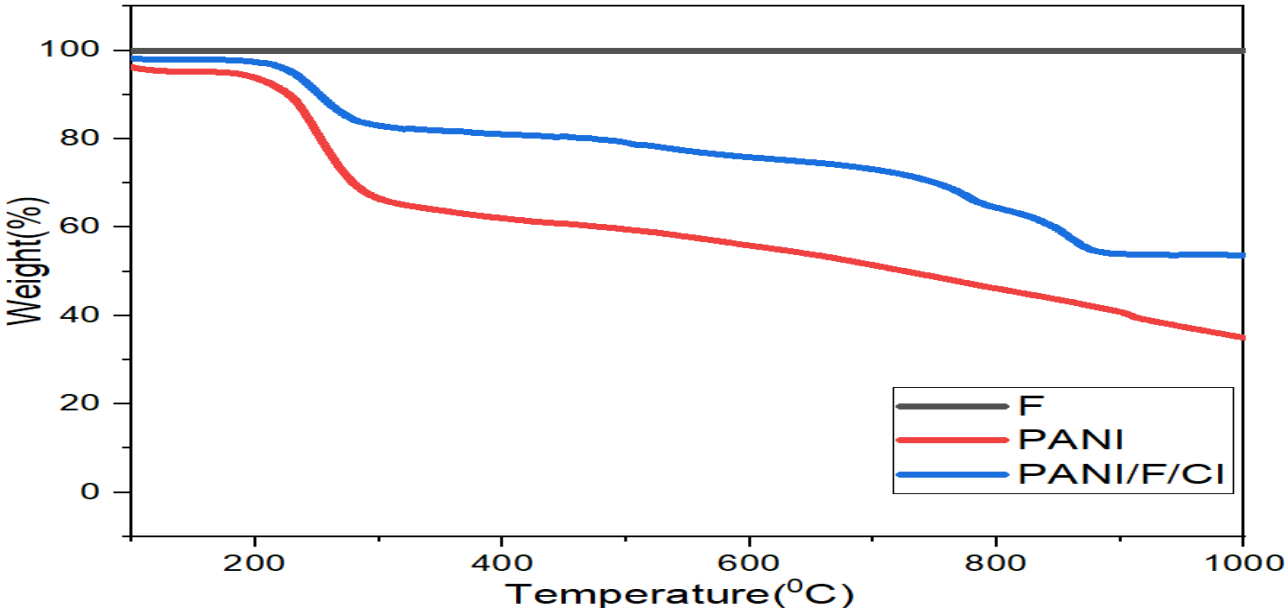

Fig. 4. TGA thermograms of $Ni_{0.5}Zn_{0.5}Fe_2O_4$, PANI/F/CI composite and pure PANI.

3.5 Morphology investigations

The morphology of the $Ni_{0.5}Zn_{0.5}Fe_2O_4$, CI, PANI and PANI/F/CI composite is shown in Fig. 5. The agglomerated spherical particles of NiZn ferrite and the spherical particles of carbonyl iron (Fig. 5a, b) are observed with the

average diameters to be ranging between 27–63 nm and 0.2–2.4 μm, respectively. While a combination of rough surface sheets and short rods connected to each other of PANI is noticed (Fig. 5 (c)), distributed in the range between 60–220 nm. On the other hand, after coating with polyaniline, a continued overlayer of PANI is created on the CI and $Ni_{0.5}Zn_{0.5}Fe_2O_4$ nanoparticles' surface (Fig. 6 (d)).

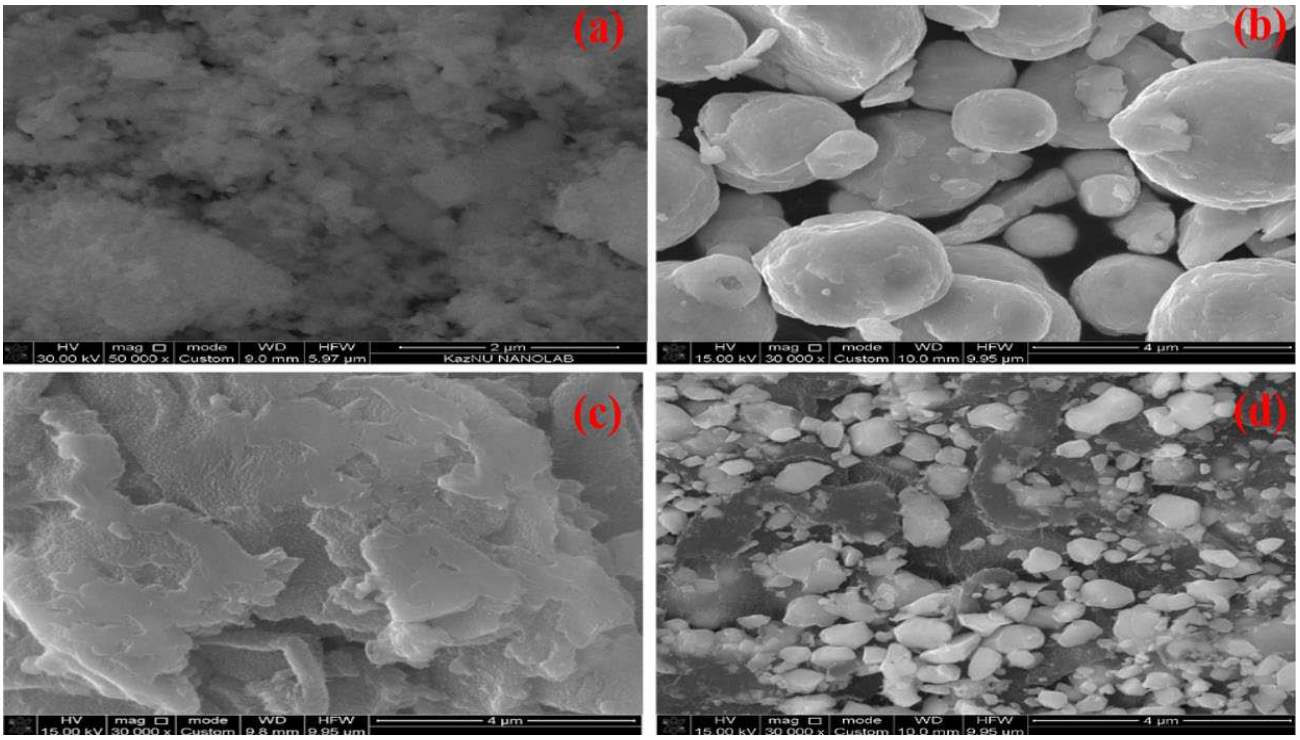

Fig. 5. SEM images of (a) $Ni_{0.5}Zn_{0.5}Fe_2O_4$, (b) CI, (c) PANI and (d) PANI/F/CI composite.

3.6 EMI shielding and MA properties

There are two general methods that cope with the interference of incident electromagnetic waves: the first one is electromagnetic interference shielding and the second one is microwave absorption. For the EMI shielding method (Fig. 6 (a)), the significant point is to attenuate the transmitted power of the EM waves (p_T). On the other hand, for the microwave absorption method (Fig. 6 (b)), though, a metal plate is put to reflect the transmitted power of the EM waves. As a consequence, the transmitted power of the EM waves is negligible in microwave absorption. EMI shielding and MA properties of the prepared samples are estimated with the free-space technique as shown in Fig. 7. EM waves are generated by a microwave generator in the frequency band of 8.8–12 GHz, where a microwave generator is connected by a WR90 waveguide instrument (IEC Standard R100, X Band). The incident EM waves (p_{in}) are measured by the horn antenna connected to an oscilloscope (Fig. 7), then the prepared sample perpendicularly is placed between a microwave generator and the horn antenna to

measure the transmitted power of the EM waves (p_T) by an oscilloscope. As a result, SE can be calculated for the EMI shielding by applying the equation (1) [28]:

$$SE\ (dB) = SE_R + SE_A + SE_M = 10\ log\frac{p_{in}}{p_T} \quad (1)$$

It is significant to note that the multiple reflection loss (SE_M) can be ignored if the absorption shielding (SE_A) of EMI shielding material is higher than 10 dB and equation (1) then can be rewritten as [28]:

$$SE\ (dB) = SE_R + SE_A = 10\ log\frac{p_{in}}{p_T} \quad (2)$$

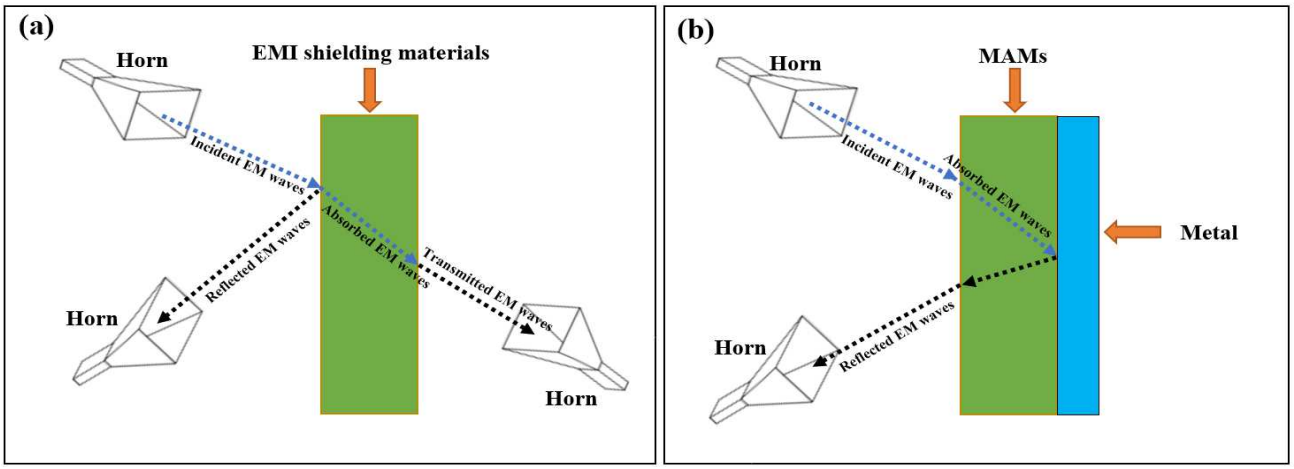

Fig. 6. Sketch of the estimate models of (a) electromagnetic interference shielding and (b) microwave absorption.

In addition to that, the reflected power of the EM waves (p_{ref}) is measured when the EM waves are incident on the sample surface at an angle of 45° by an oscilloscope. As a result, the shielding by reflection (SE_R) can be calculated for the EMI shielding by applying the equation (3):

$$SE_R\ (dB) = -10\log(1-R) = -10\log\left(1-\frac{p_{ref}}{p_{in}}\right) \quad (3)$$

Finally, the shielding by absorption (SE_A) is calculated by equation (4) [29,30]:

$$SE_A\ (dB) = -10\log\left(\frac{T}{1-R}\right) = -10\log\left(\frac{p_T}{p_{in}-p_{ref}}\right) \quad (4)$$

For the microwave absorption method, the prepared sample is placed on the metal plate at an angle of 45° to measure the reflected power of the EM waves (p_{ref}) by an oscilloscope. As a result, RL can be calculated by applying the equation (5) [29,30]:

$$Rl\ (dB) = 10log\frac{p_{in}}{p_{ref}} \quad (5)$$

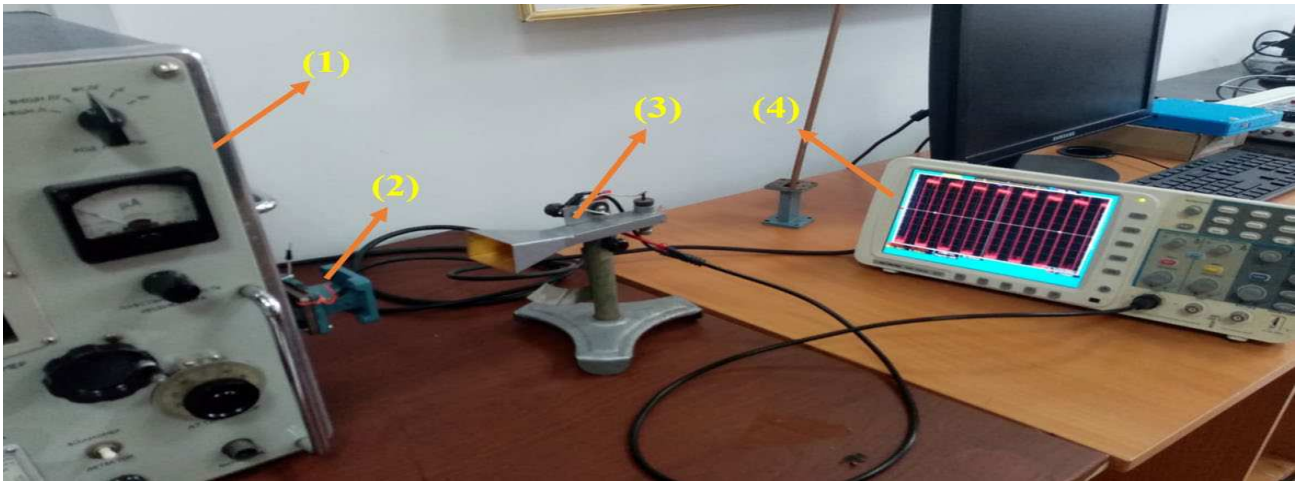

Fig. 7. Experimental setup for studying the EMI and MA properties of the prepared samples by the free-space technique. From left to right: (1) microwave generator, (2) waveguide instrument (IEC Standard R100, X Band), (3) horn antenna, and (4) oscilloscope.

3.7 Influence of the incorporation of $Ni_{0.5}Zn_{0.5}Fe_2O_4$, CI and PANI on the RL and the SE

EMI shielding and MA properties of the $Ni_{0.5}Zn_{0.5}Fe_2O_4$, CI, PANI and PANI/F/CI composite are studied. The results of this investigation are exhibited in Fig. 8, Fig. 9 and Table 1. Fig. 8 and Fig. 9 illustrate the changing of the RL and SE as a function of the EM wave frequency for $Ni_{0.5}Zn_{0.5}Fe_2O_4$, CI, PANI and PANI/F/CI composite. The absorption of samples with specified thickness at 3.2 mm is molded to measure RL and SE in the frequency band of 8.8–12.0 GHz. As illustrated in Fig. 8 and Fig. 9, for the $Ni_{0.5}Zn_{0.5}Fe_2O_4$ and CI, weak reflection loss and low shielding efficiency are noticed. On the other hand, for the pure PANI, the reflection loss is in the range between 6.6–8.5 dB and the shielding efficiency is in the range between 9.8–12.9 dB. Furthermore, when PANI is incorporated with ferrite which is mixed with carbonyl iron, the reflection loss increases to −25.8 dB at 11.3 GHz for PANI/F/CI composite and the shielding efficiency increases to 30.12 dB at 11.0 GHz. Table 1 shows the reasonable surface density (SD) of all the prepared absorbers. As a result, one can notice the impact of incorporating $Ni_{0.5}Zn_{0.5}Fe_2O_4$ and CI (magnetic loss materials) and PANI (dielectric loss material) on the EMI and MA properties of the prepared absorber. This incorporation drives an effective and low thickness absorber with a wide BW_{-10dB} [31]. Fig. 10 shows the SE_R and SE_A of the $Ni_{0.5}Zn_{0.5}Fe_2O_4$, CI, PANI and PANI/F/CI composite with a thickness of 3.2 mm at the frequency of 11.0 GHz.

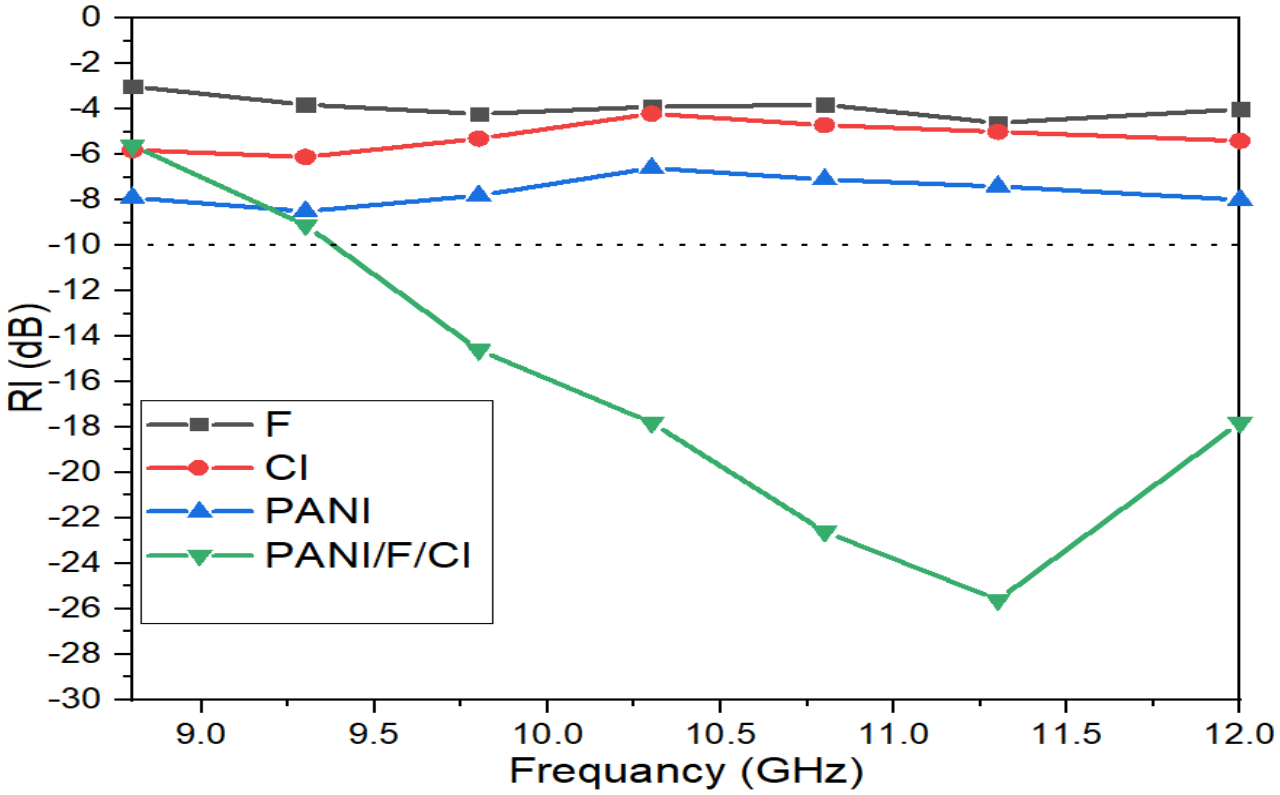

Fig. 8. RL curves of $Ni_{0.5}Zn_{0.5}Fe_2O_4$, CI, PANI and PANI/F/CI composite at 3.2 mm thickness.

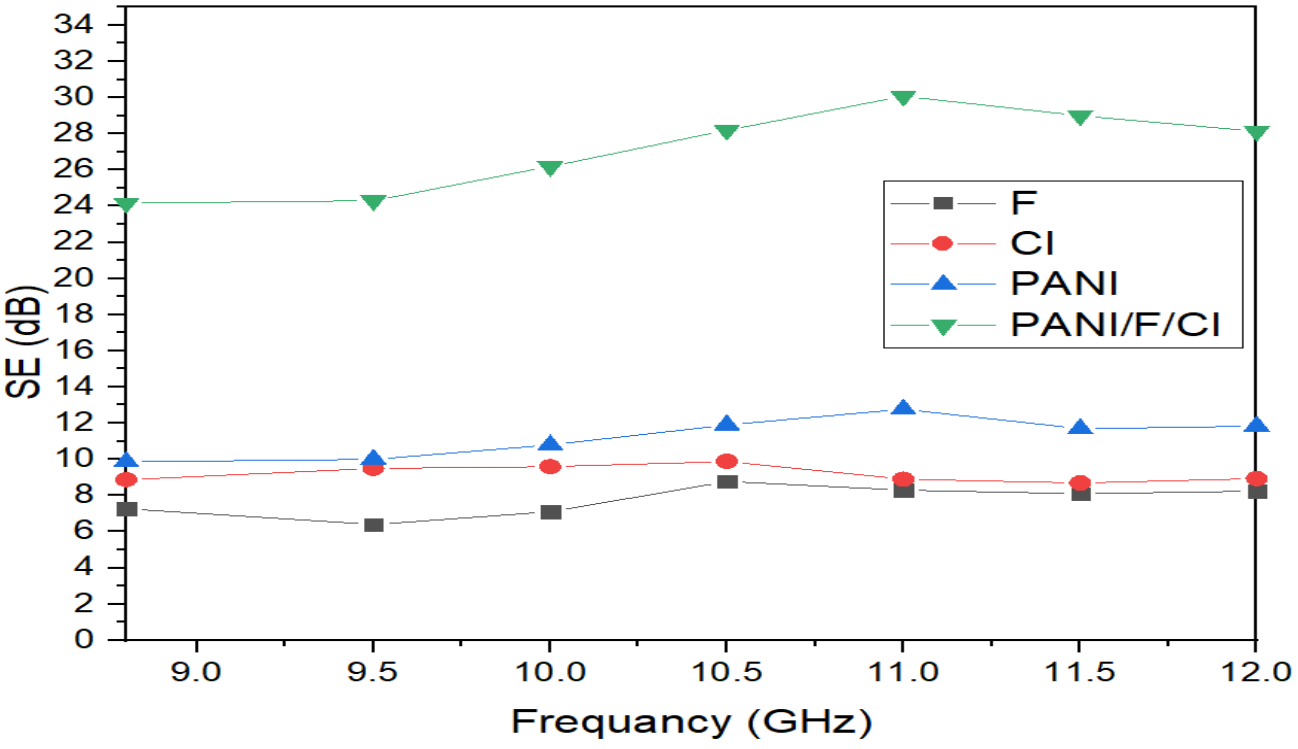

Fig. 9. SE curves of $Ni_{0.5}Zn_{0.5}Fe_2O_4$, CI, PANI and PANI/F/CI composite at 3.2 mm thickness.

Table 1. MA behavior of $Ni_{0.5}Zn_{0.5}Fe_2O_4$, CI, PANI and PANI/F/CI composite at 3.2 mm thickness.

Samples	RL_{min} (dB)	f_m (GHz)	$BW_{-10\ dB}$ (GHz)	SD (kg/m^2)
$Ni_{0.5}Zn_{0.5}Fe_2O_4$	-4.6	-	-	4.56
CI	-6.5	-	-	5.21
PANI	-8.5	-	-	2.25
PANI/F/CI	-25.7	11.3	2.6	3.31

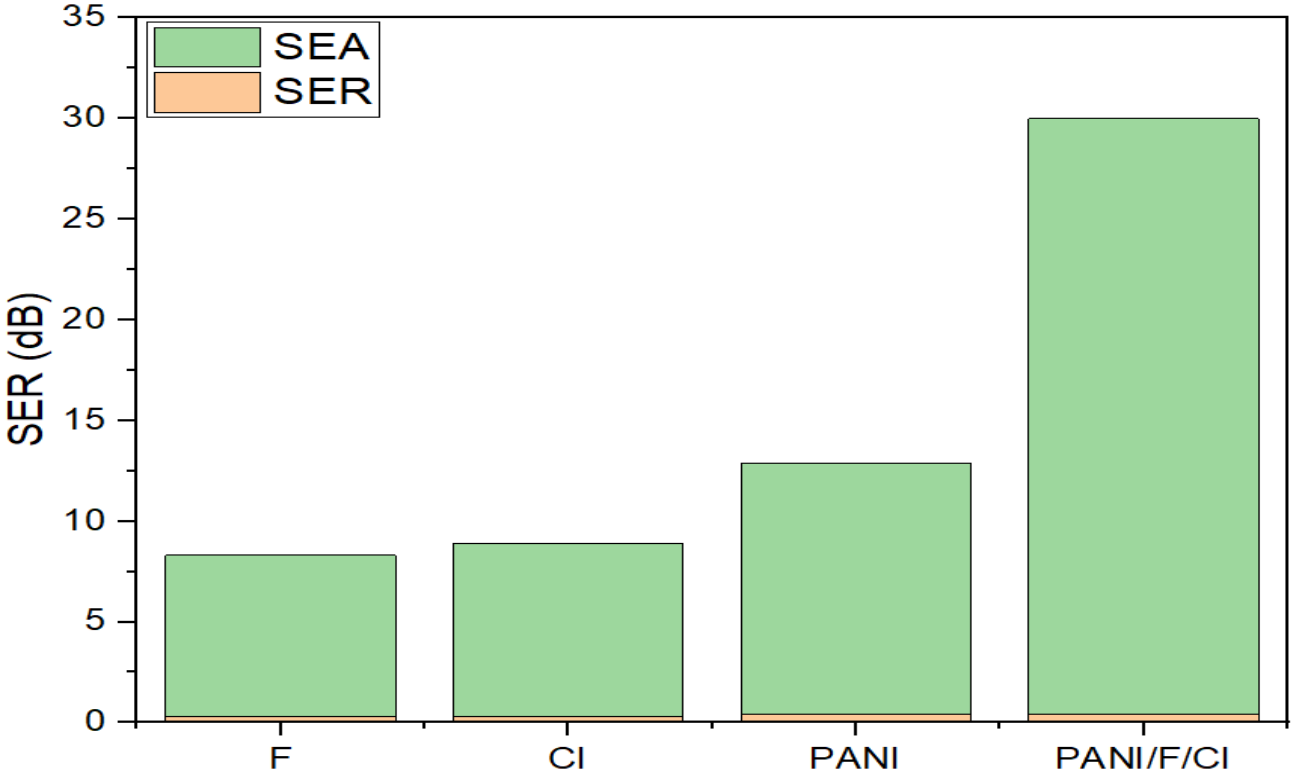

Fig. 10. Bar plot for individual components of SE_R and SE_A of $Ni_{0.5}Zn_{0.5}Fe_2O_4$, CI, PANI and PANI/F/CI composite with a thickness of 3.2 mm at the frequency of 11.0 GHz.

3.8 Influence of the PANI/F/CI composite thickness and loading ratio on the RL

Fig. 11 illustrates the RL of PANI/F/CI composite with various thicknesses (3.2, 3.4, 3.6 mm) at the various weight ratios of the absorber within a paraffin matrix (30, 35% w/w). Fig. 11 shows that the RL attenuation peaks of samples moved to lower frequencies with increasing sample thickness. This phenomenon may be defined by the quarter-wavelength (λ/4) cancellation model, as shown in equation (6) [32–34]:

$$t_m = \frac{c}{4f_m\sqrt{|\mu_r||\varepsilon_r|}} \quad (6)$$

Where $|\varepsilon_r|$ and $|\mu_r|$ are the modulus of the measured complex relative permittivity (ε_r) and permeability (μ_r) at matching frequency (f_m), respectively. c is the velocity of light.

It can be noticed from equation (6) that the f_m is inversely proportionate to the thickness of an absorber. On the other hand, one can notice the minimum reflection loss moves gradually to a lower frequency with the increase in weight ratios of the absorber within a paraffin matrix (Fig. 11). Furthermore, Table 2 shows the PANI/F/CI composites have reasonable surface density, ranging from 3.31 to 3.40 kg/m^2, and wide bandwidth extending from 2.5 to 3.0 GHz. One can conclude that the optimal absorption can be accomplished by modifying the absorber thickness and the loading ratio of the absorber within a paraffin matrix.

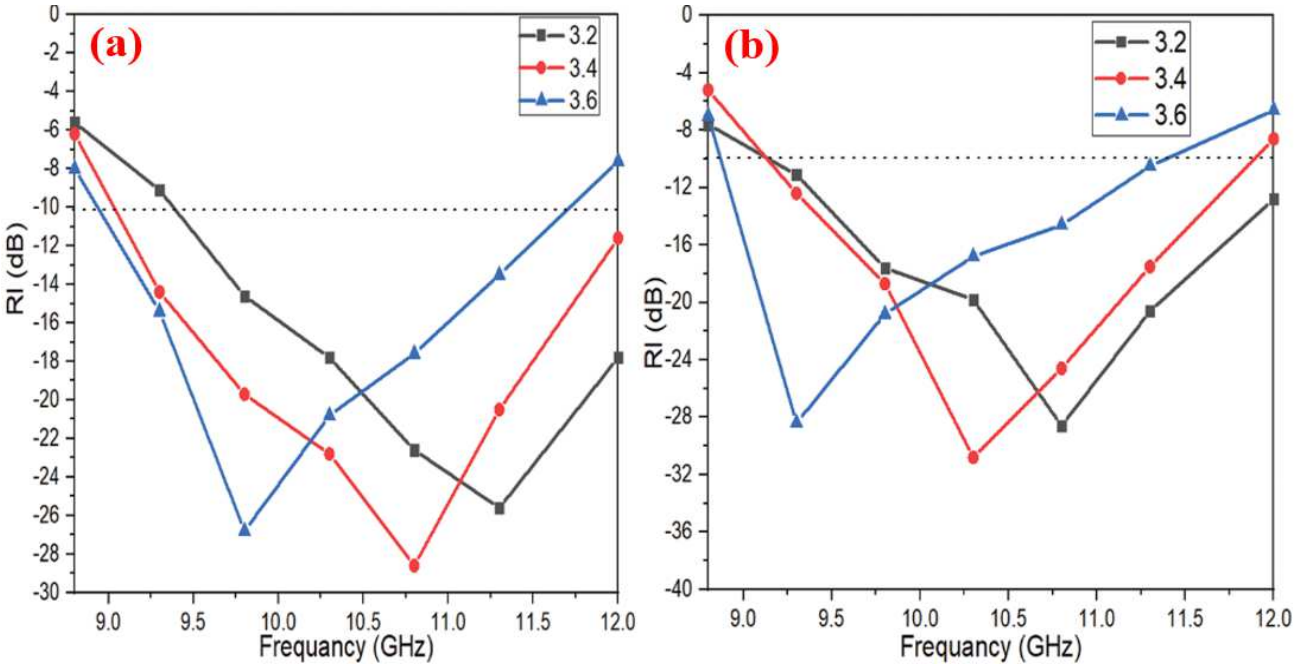

Fig. 11. RL curves of PANI/F/CI composite with various thicknesses (3.2, 3.4, 3.6 mm) at the various weight ratios of the absorber within a paraffin matrix (a) 30% and (b) 35%.

Table 2. MA behavior of PANI/F/CI composite at various thicknesses and various loading ratios within a paraffin matrix.

Loading ratio %	t (mm)	RL_{min} (dB)	f_m (GHz)	BW_{-10dB} (GHz)	SD (kg/m^2)
30%	3.2	-25.7	11.3	2.6	3.31
	3.4	-28.5	10.8	3.0	3.35
	3.6	-26.8	9.8	2.9	3.37
35%	3.2	-28.6	10.8	2.5	3.33
	3.4	-30.8	10.3	2.8	3.38
	3.6	-28.4	9.3	2.6	3.40

4. Conclusion

In the current research, PANI/F/CI microwave absorbers were successfully synthesized and characterized by XRD, FTIR spectroscopy, UV–vis spectroscopy, TGA analysis and SEM analysis. The functional characterization was accomplished by measuring the EMI shielding and MA properties. $Ni_{0.5}Zn_{0.5}Fe_2O_4$ and CI were used to enhance the mechanism of magnetic loss, while PANI was introduced to enhance the mechanism of dielectric loss. As a result, one can notice the impact of combining $Ni_{0.5}Zn_{0.5}Fe_2O_4$, CI and PANI on the EMI and MA properties of the absorber. This combination drives an effective and low thickness absorber with minimal reflection loss. The results refer that the optimal absorption can be accomplished by modifying the absorber thickness and the loading ratio of the absorber within a paraffin matrix. Minimal reflection loss of -30.8 dB at the matching frequency of 10.3 GHz and the absorption bandwidth under -10 dB of 2.8 GHz for 3.4 mm thickness with a surface density of 3.38 kg/m^2 were noticed for the PANI/F/CI microwave absorber. The maximum shielding efficiency of 30.12 dB at 11.0 GHz for 3.2 mm thickness was observed for the PANI/F/CI microwave absorber.

Acknowledgments

The authors express their gratitude to Al-Farabi Kazakh National University, the center of complex processing of mineral raw materials, and the center of physical-chemical methods of research and analyses for providing the materials and equipment to conduct this research project.

References

[1] H. Lv, Z. Yang, S.J.H. Ong, C. Wei, H. Liao, S. Xi, Y. Du, G. Ji, Z.J. Xu, A Flexible Microwave Shield with Tunable Frequency-Transmission and Electromagnetic Compatibility, Adv. Funct. Mater. 29 (2019) 1–8. https://doi.org/10.1002/adfm.201900163.

[2] C. Liang, H. Qiu, P. Song, X. Shi, J. Kong, J. Gu, Ultra-light MXene aerogel/wood-derived porous carbon composites with wall-like "mortar/brick" structures for electromagnetic interference shielding, Sci. Bull. 65 (2020) 616–622. https://doi.org/10.1016/j.scib.2020.02.009.

[3] X. Chen, T. Shi, K. Zhong, G. Wu, Y. Lu, Capacitive behavior of MoS2 decorated with FeS2@carbon nanospheres, Chem. Eng. J. 379 (2020). https://doi.org/10.1016/j.cej.2019.122240.

[4] S. Chen, G. Meng, B. Kong, B. Xiao, Z. Wang, Z. Jing, Y. Gao, G. Wu, H. Wang, Y. Cheng, Asymmetric alicyclic amine-polyether amine molecular chain structure for improved energy storage density of high-temperature crosslinked polymer capacitor, Chem. Eng. J. 387 (2020) 123662. https://doi.org/10.1016/j.cej.2019.123662.

[5] C. Cheng, Z. Chen, Z. Huang, C. Zhang, R. Tusiime, J. Zhou, Z. Sun, Y. Liu, M. Yu, H. Zhang, Simultaneously improving mode I and mode II fracture toughness of the carbon fiber/epoxy composite laminates via interleaved with uniformly aligned PES fiber webs, Compos. Part A Appl. Sci. Manuf. 129 (2020) 105696. https://doi.org/10.1016/j.compositesa.2019.105696.

[6] H. Xu, X. Yin, X. Li, M. Li, S. Liang, L. Zhang, L. Cheng, Lightweight Ti 2 CT x MXene/Poly(vinyl alcohol) Composite Foams for Electromagnetic Wave Shielding with Absorption-Dominated Feature, ACS Appl. Mater. Interfaces. 11 (2019) 10198–10207. https://doi.org/10.1021/acsami.8b21671.

[7] Y. Liu, X. Liu, X. Wang, Synthesis and microwave absorption properties of Ni-Zn-Mn spinel ferrites, Adv. Appl. Ceram. 114 (2015) 82–86. https://doi.org/10.1179/1743676114Y.0000000194.

[8] W. Ari Adi, Y. Yunasfi, M. Mashadi, D. Sahidin Winatapura, A. Mulyawan, Y. Sarwanto, Y. Edi Gunanto, Y. Taryana, Metamaterial: Smart Magnetic Material for Microwave Absorbing Material, Electromagn. Fields Waves. (2019) 1–18. https://doi.org/10.5772/intechopen.84471.

[9] P.J. Liu, Z.J. Yao, V.M.H. Ng, J.T. Zhou, Z.H. Yang, L.B. Kong, Enhanced microwave absorption properties of double-layer absorbers based on spherical NiO and Co0.2Ni0.4Zn0.4Fe2O4 ferrite composites, Acta Metall. Sin. (English Lett. 31 (2018) 171–179. https://doi.org/10.1007/s40195-017-0612-5.

[10] T. Indrusiak, I.M. Pereira, A.P. Heitmann, J.G. Silva, Â.M.L. Denadai, B.G. Soares, Epoxy/ferrite nanocomposites as microwave absorber materials: effect of multilayered structure, J. Mater. Sci. Mater. Electron. (2020). https://doi.org/10.1007/s10854-

020-03863-0.

[11] T.H. Ting, R.P. Yu, Y.N. Jau, Synthesis and microwave absorption characteristics of polyaniline/NiZn ferrite composites in 2-40 GHz, Mater. Chem. Phys. 126 (2011) 364–368. https://doi.org/10.1016/j.matchemphys.2010.11.011.

[12] A. Houbi, Z.A. Aldashevich, Y. Atassi, Z. Bagasharova Telmanovna, M. Saule, K. Kubanych, Microwave absorbing properties of ferrites and their composites: A review, J. Magn. Magn. Mater. 529 (2021) 167839. https://doi.org/10.1016/j.jmmm.2021.167839.

[13] Design of lightweight broadband microwave absorbers in the X-band.pdf, (n.d.).

[14] C.P. Wang, C.H. Li, H. Bi, J.C. Li, H. Zhang, A.J. Xie, Y.H. Shen, Novel one-dimensional polyaniline/Ni0.5Zn0.5Fe2O4 hybrid nanostructure: Synthesis, magnetic, and electromagnetic wave absorption properties, J. Nanoparticle Res. 16 (2014). https://doi.org/10.1007/s11051-014-2289-2.

[15] M. Wang, G. Ji, B. Zhang, D. Tang, Y. Yang, Y. Du, Controlled synthesis and microwave absorption properties of Ni0.6Zn0.4Fe2O4/PANI composite via an in-situ polymerization process, J. Magn. Magn. Mater. 377 (2015) 52–58. https://doi.org/10.1016/j.jmmm.2014.10.066.

[16] A.M. El Nahrawy, H.S. El-Deen, A.A. Soliman, W.M.M. Mosa, Crystallographic and magnetic properties of Al3+co-doped NiZnFe2O4 nano-particles prepared by sol-gel process, Egypt. J. Chem. 62 (2019) 925–932. https://doi.org/10.21608/EJCHEM.2018.4504.1397.

[17] N. Bahri-Laleh, K. Didehban, E. Yarahmadi, S.A. Mirmohammadi, G. Wang, Microwave Absorption Properties of Polyaniline/Carbonyl Iron Composites, Silicon. 10 (2018) 1337–1343. https://doi.org/10.1007/s12633-017-9609-y.

[18] S.N. Ezzati, M. Rabbani, R.M. Leblanc, E. Asadi, S.M.H. Ezzati, R. Rahimi, S. Azodi-Deilami, Conducting, magnetic polyaniline/Ba0.25Sr0.75Fe11(Ni0.5Mn0.5)O19 nanocomposite: Fabrication, characterization and application, J. Alloys Compd. 646 (2015) 1157–1164. https://doi.org/10.1016/j.jallcom.2015.05.146.

[19] X. Meng, Y. Zhu, S. Xu, T. Liu, Facile synthesis of shell-core polyaniline/SrFe12O19 composites and magnetic properties, RSC Adv. 6 (2016) 4946–4949. https://doi.org/10.1039/c5ra22200a.

[20] N.N. Ali, Y. Atassi, A. Salloum, A. Charba, A. Malki, M. Jafarian, Comparative study of microwave absorption characteristics of (Polyaniline/NiZn ferrite) nanocomposites with different ferrite percentages, Mater. Chem. Phys. 211 (2018) 79–87. https://doi.org/10.1016/j.matchemphys.2018.02.017.

[21] A.H. Elsayed, M.S.M. Eldin, A.M. Elsyed, A.H.A. Elazm, E.M. Younes, Synthesis and Properties of Polyaniline / ferrites Nanocomposites, 6 (2011) 206–221.

[22] S.B. Kondawar, A.I. Nandapure, Magnetic and electrical properties of zinc-substituted nickel ferrite reinforced conducting polyaniline nanocomposites, J. Chinese Adv. Mater. Soc. 2 (2014) 186–198. https://doi.org/10.1080/22243682.2014.934919.

[23] S.J. Figueroa Ramírez, M. Miranda-Hernánde, Carbon film electrodes as support of metallic particles, Int. J. Electrochem. Sci. 7 (2012) 150–166.

[24] S.Y. Kim, S.H. Kwon, Y.D. Liu, J.S. Lee, C.Y. You, H.J. Choi, Core-shell-structured cross-linked poly(glycidyl methacrylate)-coated carbonyl iron microspheres and their magnetorheology, J. Mater. Sci. 49 (2014) 1345–1352. https://doi.org/10.1007/s10853-013-7818-3.

[25] S.P. Gairola, V. Verma, L. Kumar, M.A. Dar, S. Annapoorni, R.K. Kotnala, Enhanced microwave absorption properties in polyaniline and nano-ferrite composite in X-band, Synth. Met. 160 (2010) 2315–2318. https://doi.org/10.1016/j.synthmet.2010.08.025.

[26] G. Li, S. Yan, E. Zhou, Y. Chen, Preparation of magnetic and conductive NiZn ferrite-polyaniline nanocomposites with core-shell structure, Colloids Surfaces A Physicochem. Eng. Asp. 276 (2006) 40–44. https://doi.org/10.1016/j.colsurfa.2005.10.010.

[27] L. Li, J. Jiang, F. Xu, Synthesis and ferrimagnetic properties of novel Sm-substituted LiNi ferrite-polyaniline

nanocomposite, Mater. Lett. 61 (2007) 1091–1096. https://doi.org/10.1016/j.matlet.2006.06.061.

[28] P. Verma, T. Bansala, S.S. Chauhan, D. Kumar, S. Deveci, S. Kumar, Electromagnetic interference shielding performance of carbon nanostructure reinforced, 3D printed polymer composites, J. Mater. Sci. 56 (2021) 11769–11788. https://doi.org/10.1007/s10853-021-05985-0.

[29] M. Bayat, H. Yang, F.K. Ko, D. Michelson, A. Mei, Electromagnetic interference shielding effectiveness of hybrid multifunctional Fe3O4/carbon nanofiber composite, Polymer (Guildf). 55 (2014) 936–943. https://doi.org/10.1016/j.polymer.2013.12.042.

[30] Y.K. Hong, C.Y. Lee, C.K. Jeong, D.E. Lee, K. Kim, J. Joo, Method and apparatus to measure electromagnetic interference shielding efficiency and its shielding characteristics in broadband frequency ranges, Rev. Sci. Instrum. 74 (2003) 1098–1102. https://doi.org/10.1063/1.1532540.

[31] N.N. Ali, Y. Atassi, A. Salloum, A. Malki, M. Jafarian, R.K.B. Almarjeh, Lightweight broadband microwave absorbers of core–shell (polypyrrole/NiZn ferrite) nanocomposites in the X-band: insights on interfacial polarization, J. Mater. Sci. Mater. Electron. 30 (2019) 6876–6887. https://doi.org/10.1007/s10854-019-01002-y.

[32] S. Wang, Q. Jiao, Q. Shi, H. Zhu, T. Feng, Q. Lu, C. Feng, H. Li, D. Shi, Y. Zhao, Synthesis of porous nitrogen-doped graphene decorated by γ-Fe2O3 nanorings for enhancing microwave absorbing performance, Ceram. Int. 46 (2020) 1002–1010. https://doi.org/10.1016/j.ceramint.2019.09.064.

[33] R. Shu, J. Zhang, C. Guo, Y. Wu, Z. Wan, J. Shi, Y. Liu, M. Zheng, Facile synthesis of nitrogen-doped reduced graphene oxide/nickel-zinc ferrite composites as high-performance microwave absorbers in the X-band, Chem. Eng. J. 384 (2020) 123266. https://doi.org/10.1016/j.cej.2019.123266.

[34] R. Jaiswal, K. Agarwal, R. Kumar, R. Kumar, K. Mukhopadhyay, N.E. Prasad, EMI and microwave absorbing efficiency of polyaniline-functionalized reduced graphene oxide/γ-Fe2O3/epoxy

nanocomposite, Soft Matter. 16 (2020)
6643–6653.
https://doi.org/10.1039/d0sm00266f.